# Oral Treatment with the D-Enantiomeric Peptide D3 Improves the Pathology and Behavior of Alzheimer's Disease Transgenic Mice

Susanne Aileen Funke,[†,⊗] Thomas van Groen,[‡,§,⊗] Inga Kadish,[‡,§] Dirk Bartnik,[∥] Luitgard Nagel-Steger,[∥] Oleksandr Brener,[∥] Torsten Sehl,[∥] Renu Batra-Safferling,[⊥] Christine Moriscot,[#,▽,○,♦] Guy Schoehn,[#,▽,○,♦] Anselm H. C. Horn,[¶] Andreas Müller-Schiffmann,[+] Carsten Korth,[+] Heinrich Sticht,[¶] and Dieter Willbold*[,†,∥,#]

[†]Forschungszentrum Jülich, ISB-3, 52425 Jülich, Germany, [‡]Department of Cell Biology, University of Alabama at Birmingham, Birmingham, Alabama 35294, [§]Department of Neurobiology, University of Alabama at Birmingham, Birmingham, Alabama 35294, [∥]Heinrich-Heine-Universität Düsseldorf, Institut für Physikalische Biologie and BMFZ, 40225 Düsseldorf, Germany, [⊥]Forschungszentrum Jülich, ISB-2, 52425 Jülich, Germany, [#]CEA, [▽]CNRS, and [○]Université Joseph Fourier, Institut de Biologie Structurale Jean-Pierre Ebel, UMR5075 Grenoble, France, [♦]Unit for Virus Host Cell Interactions, 6, rue Jules Horowitz BP 181, F38042 Grenoble, France, [¶]Friedrich-Alexander-Universität Erlangen-Nürnberg, Institut für Biochemie, 91054 Erlangen, Germany, and [+]Heinrich-Heine-Universität Düsseldorf, Institut für Neuropathologie, 40225 Düsseldorf, Germany

## Abstract

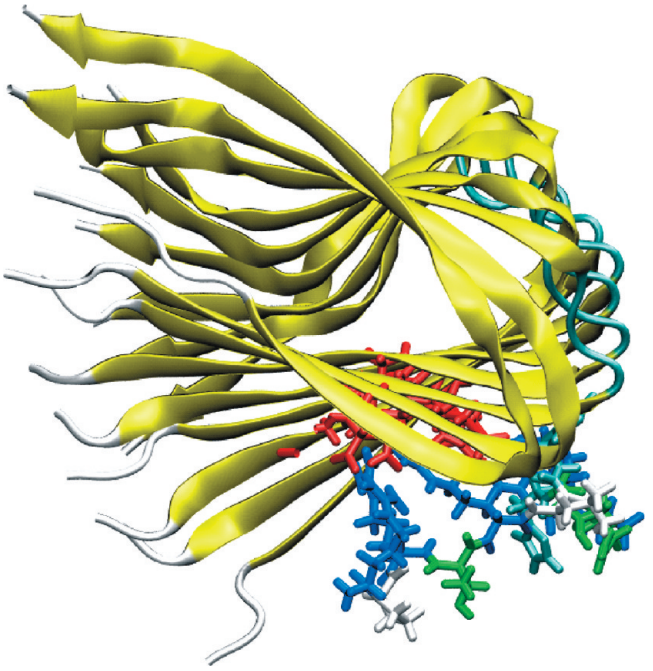

Several lines of evidence suggest that the amyloid-$\beta$-peptide (A$\beta$) plays a central role in the pathogenesis of Alzheimer's disease (AD). Not only A$\beta$ fibrils but also small soluble A$\beta$ oligomers in particular are suspected to be the major toxic species responsible for disease development and progression. The present study reports on in vitro and in vivo properties of the A$\beta$ targeting D-enantiomeric amino acid peptide D3. We show that next to plaque load and inflammation reduction, oral application of the peptide improved the cognitive performance of AD transgenic mice. In addition, we provide in vitro data elucidating the potential mechanism underlying the observed in vivo activity of D3. These data suggest that D3 precipitates toxic A$\beta$ species and converts them into nonamyloidogenic, nonfibrillar, and nontoxic aggregates without increasing the concentration of monomeric A$\beta$. Thus, D3 exerts an interesting and novel mechanism of action that abolishes toxic A$\beta$ oligomers and thereby supports their decisive role in AD development and progression.

**Keywords:** Mirror image phage display, D-enantiomeric peptide, Alzheimer's disease, oligomers, drugs

Alzheimer's disease (AD) is a progressive neurodegenerative disorder, affecting more than 27 million people worldwide (*1*). Several lines of research have provided strong evidence of a central role played by amyloid-$\beta$-peptide (A$\beta$) in the pathogenesis of AD. A$\beta$ is produced normally and throughout life as a 39−43 residue peptide from the amyloid precursor protein (APP) by two distinct proteolytic activities, called $\beta$- and $\gamma$-secretases (*2*−*4*). Histopathological hallmarks of AD are aggregated protein deposits (i.e., senile plaques and neurofibrillary tangles) in the brain. Senile plaques consist mainly of A$\beta$. According to the amyloid cascade hypothesis, fibrillar forms of A$\beta$ have been thought to be responsible for neuronal dysfunction (*5*, *6*). More recent studies indicate that diffusable A$\beta$ oligomers, including protofibrils, prefibrillar aggregates, and ADDLs, are the major toxic species during disease development and progression (*7*−*10*). Therefore, agents that interfere with early A$\beta$ oligomerization are expected to be especially valuable for use in the therapy or prevention of AD. In turn, if such

**Received Date:** June 11, 2010
**Accepted Date:** July 21, 2010
**Published on Web Date:** August 02, 2010



DOI: 10.1021/cn100057j | *ACS Chem. Neurosci.* (2010), *1*, 639–648

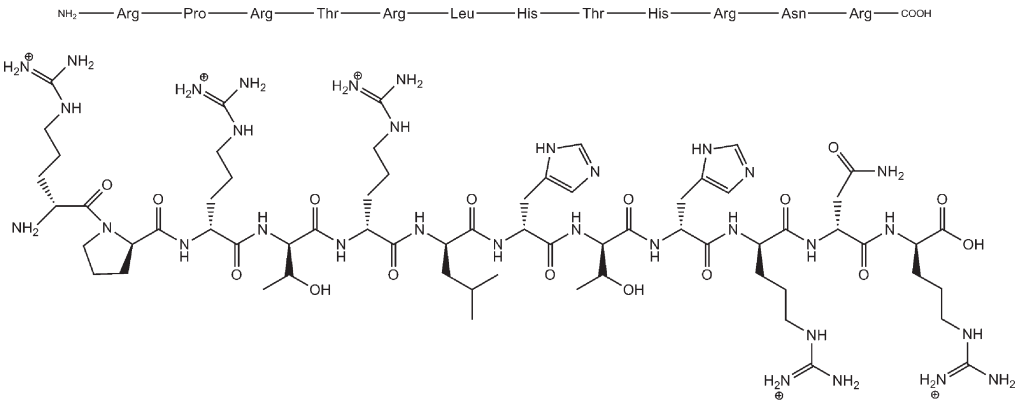


**Figure 1.** Lewis structure of the D-enantiomeric peptide D3.

agents prove to be effective in therapy or the prevention of AD, they would further strengthen the role of A$\beta$ oligomers for disease development and progression.

So far, only palliative therapies for AD are available. Acetylcholine inhibitors such as Donepezil, Galantamine, and the NMDA receptor antagonist Memantine have been approved for clinical use in the treatment of cognitive symptoms (*11*, *12*). Approaches targeting A$\beta$ include the reduction of A$\beta$ production by inhibitors or modulators of the $\beta$- or $\gamma$-secretases, A$\beta$ vaccination, and interference of A$\beta$ aggregation by small molecules or peptides (*13*, *14*). A variety of such substances have already been described, e.g., Congo red (*15*), scyllo-Inositol (*16*, *17*), amino-propane sulfonic acid (*18*), Clioquinol (*19*, *20*), methylene blue (*21*), polyphenol (−)-epigallocatechin (EGCG) (*22*, *23*), and oligomeric acylated aminopyrazoles (*24*, *25*).

Small peptides that inhibit the aggregation of A$\beta$ and reduce its toxic effects have also been identified and a fraction of them shown to be effective in AD transgenic mice (*26*−*29*). Recently, a $\beta$-sheet breaking D-enantiomeric dipeptide was reported to selectively target A$\beta$ soluble oligomers. The compound was orally bioavailable, reduced the plaque load in AD transgenic mice, and improved their cognitive performance (*30*).

Earlier, we reported the identification of A$\beta$42 binding D-enantiomeric 12-mer peptides by mirror image phage display selections (*31*−*34*). Such D-peptides are known to be extremely protease resistant, thus being potentially well-suited for in vivo use (*35*, *36*). The D-peptide D3 (amino acid sequence RPRTRLHTHRNR, Figure 1) was identified during a mirror image phage display selection using D-enantiomeric A$\beta$42 as a target under conditions where monomeric or small oligomeric A$\beta$42 species can be expected to be the dominating species. In vitro, D3 inhibits the formation of regular A$\beta$ fibrils and reduces A$\beta$42 cytotoxicty. In vivo, D3 reduces plaque load and cerebral inflammation of transgenic mouse models of AD upon direct application into the brain (*32*). The present study aims to investigate the effect of orally applied D3 on plaque load and on the cognitive behavior of AD transgenic mice. In addition, various in vitro experiments were carried out to elucidate the potential mechanism of D3 action.

## Results and Discussion

The APP-PS mouse model expressing human APPswe and PS1-$\Delta$E9 develops elevated levels of A$\beta$42 at the age of about four months, and at around 5 months of age, it shows typical A$\beta$ plaques (*37*). Young, four-month old female mice were orally treated with D3 by adding D3 to the drinking water for eight weeks. Depending on the water uptake, the mice consumed between 0.5 and 1 mg/day D3. Another group of mice was unilaterally infused in the hippocampus for eight weeks using Alzet minipumps. The amount of D3 totally applied per mouse was 0.5 mg. As a control, the third group was implanted with empty Alzet minipumps. After 7 weeks of D3 treatment, all groups of mice were tested in the Morris water maze. The D3 treated mice showed a significant improvement of learning during the week of testing, but the untreated mice did not (Figure 2A). Interestingly, the orally treated mice performed better in the water maze than the brain infused ones, probably due to the higher amount of applied D3. After the completion of the behavioral testing, the animals were sacrificed and the brains assessed for AD pathology. In the sections that were stained for human A$\beta$(4−10) immunoreactivity, the total A$\beta$ load in the hippocampus and frontal cortex was measured. Brain tissue sections of D3 treated mice had a significantly lower A$\beta$ load as compared to that of the untreated mice (Figure 2B,C), very similar to those treated with D3 at the age of eight months via direct infusion into the brain (*32*). Analysis of brain sections stained for GFAP or microglia revealed that D3 treatment did not cause any significant inflammation or obvious pathology. A more detailed analysis of the magnitude of inflammation near A$\beta$ deposits even revealed a significant reduction of plaque-related inflammation (measured in both GFAP and CD11b staining) in orally treated mice as compared to that in untreated and brain infused mice (Table 1).



DOI: 10.1021/cn100057j | ACS Chem. Neurosci. (2010), 1, 639–648

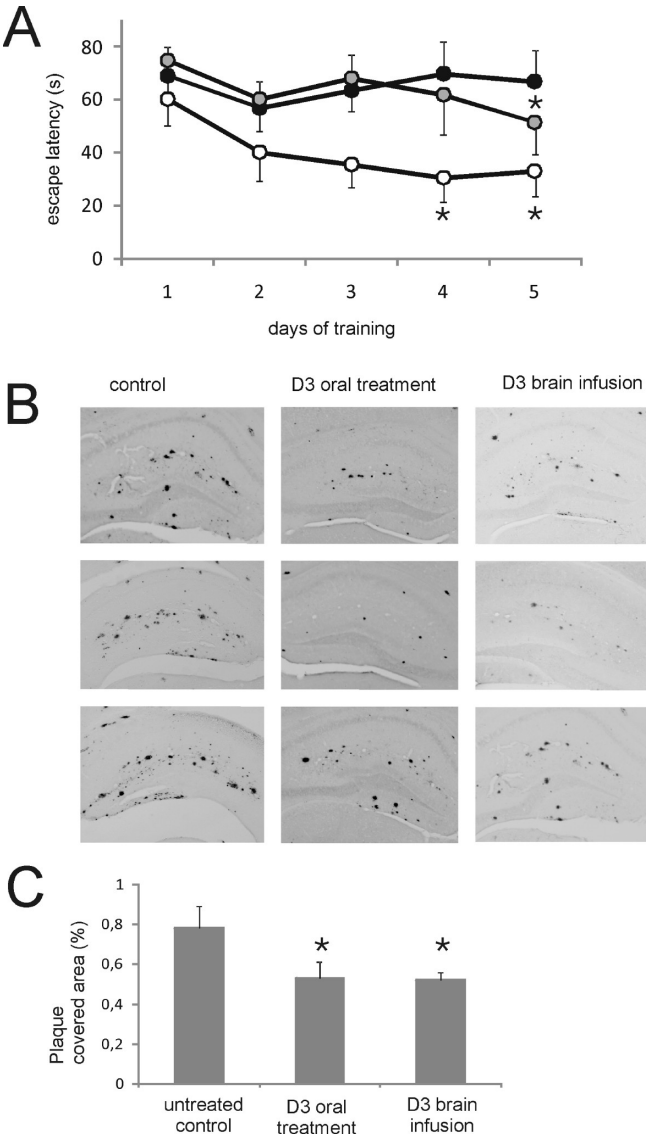


**Figure 2.** Results of the transgenic animal studies. (A) Time needed to find the hidden platform in the Morris water maze assay by the mice that were treated with D3 added to the drinking water (open circles), by direct brain infusion of D3 (gray filled circles), or not treated (black filled circles). For details see the Methods section. Error bars indicate standard deviations. (B) Photomicrographs of coronal sections of the hippocampus stained for A$\beta$ (W0−2 antibody) from control mice (left column), orally D3 treated mice (middle column), and mice treated by brain infusion (right column). (C) Quantitative evaluation of A$\beta$ plaque load. Bars indicate the A$\beta$ plaque load (area covered by A$\beta$) in the dorsal hippocampus of D3 treated and untreated mice. * indicates significantly different, $p < 0.05$.

Because of the very different amounts of applied D3, the data of the orally treated mice (up to 1 mg/day) are difficult to compare with the data of the mice that were treated by direct infusion into the brain (9 $\mu$g/day). Therefore, the complete oral application assay was repeated, applying smaller amounts of D3. This time, D3 was not added to the drinking water. Instead, implanted Alzet minipumps delivered exact amounts (0.1 mg/day) of saline solved D3 directly into the stomach of the treated group of mice ($n = 8$). A control group ($n = 9$) was treated with saline. The applied amounts of D3 were 5- to 10-fold less than that in the drinking water assay. Nevertheless, the differences between treated and control groups concerning behavior and inflammation were significant (Supporting Information, Table S1 and Figure S1).

Currently, it is critically discussed, whether the reduction of A$\beta$ fibrils in plaques at the cost of augmenting oligomer A$\beta$ assemblies could be harmful. Therefore, it was important to elucidate the potential mechanism of D3 action. To do this, we performed various assays to investigate the effects of D3 on A$\beta$ in vitro.

A method suitable to investigate the effect of D3 on the size distribution of A$\beta$ particles is dynamic light scattering (DLS). Therefore, solutions containing 5 $\mu$M A$\beta$ with and without D3 were assayed to estimate the size of A$\beta$ particles and their development over time. In the absence of D3, the A$\beta$ solution revealed a very dominating particle species with an averaged hydrodynamic radius (RH) of 30 nm over a time period of 10 min (Figure 3A), a result that is consistent with other studies (*38*). In the presence of D3, additional particles with sizes of 80 and 700 nm were observed after less than 10 min. This suggests that D3 induces the formation of huge A$\beta$ particles. D3 alone as a control did not develop any detectable particles. D3 induced formation of large A$\beta$ particles was confirmed by size exclusion chromatography (SEC) and turbidity assays (see Supporting Information, Figures S2 and S3).

A$\beta$ species can be separated from each other according to their size using density gradient centrifugation on preformed gradients of iodixanol (*25*). To further investigate the effects of D3 on A$\beta$ particle size, 125 $\mu$M A$\beta$42 samples with and without D3 (1:1) were analyzed by density gradient centrifugation runs. After centrifugation, 14 fractions of 140 $\mu$L each were harvested and analyzed for A$\beta$ content by SDS−PAGE analysis and subsequent silver staining (Figure 3B). In the absence of D3, the A$\beta$42 species are broadly distributed over nearly all fractions, corresponding to all possible A$\beta$ particle sizes with a maximum found in fractions 11 and 12 corresponding to fibrillar aggregates. Samples containing D3 had a drastically reduced A$\beta$ content in fractions 4 to 11. Calibration with proteins of known s-values indicated that these fractions contained A$\beta$ aggregates with s-values in the range of 6.5 to 18 S. Assuming a globular shape as a rough estimation, those species correspond to A$\beta$ 16 to 200-mers. Obviously, the presence of D3 resulted in the loss of oligomers and increased A$\beta$ contents in fractions corresponding to very high molecular weights (Figure 3B, fractions 12 and 14). The large-sized A$\beta$ aggregates in samples containing D3 showed neither a positive ThT signal nor amyloid properties upon staining with Congo red, indicating the absence of regular fibrils.



DOI: 10.1021/cn100057j | *ACS Chem. Neurosci.* (2010), *1*, 639–648

**Table 1.** Summary of Important Quantities: Number of Animals Per Group, Body Weight, the Aβ Load, the Number of Congo Red Positive Plaques, and the Density of Staining for the GFAP and Microglia around Plaques in the Dorsal Hippocampus[a]

| group | control | D3 brain infusion | D3 oral treatment |
|---|---|---|---|
| treatment | empty Alzet minipump | D3, brain infused by Alzet minipump | D3 added to drinking water |
| peptide amount [mg/day] | | 0.009 | 0.5−1.0 |
| number | $n = 6$ | $n = 6$ | $n = 6$ |
| body weight [g] | 23.8 ± 0.6 | 23.4 ± 0.9 | 23.1 ± 0.6 |
| swim speed [cm/s] | 17.04 ± 0.88 | 16.12 ± 1.72 | 15.91 ± 1.21 |
| probe trial [s in quadrant] | L 12.68 ± 2.40 | L 17.47 ± 3.24 | L 13.75 ± 1.84 |
| | C 20.08 ± 2.69 | C 20.70 ± 5.14 | C 18.99 ± 2.25 |
| | A 9.80 ± 1.79 | A 10.13 ± 3.26 | A 12.28 ± 2.06 |
| | R 17.60 ± 2.04 | R 11.87 ± 2.56 | R 14.62 ± 1.77 |
| Aβ plaque load [%] | 0.78 ± 0.11 | 0.53 ± 0.04* | 0.53 ± 0.08%* |
| Congo red | 12.9 ± 2.5 | 11.8 ± 1.5 | 7.5 ± 2.0* |
| GFAP | 98.6 ± 2.7 | 96.5 ± 3.1 | 86.4 ± 3.2* |
| microglia | 136 ± 3.5 | 132 ± 3.8 | 112 ± 4.3* |

[a] L, left; C, correct; A, across; R, right. * indicates significantly different, $p < 0.05$.

Indeed, electron microscopic (EM) analysis (Figure 4A,B) revealed Aβ typical fibrils (twisted ribbons) and spherical particles in the Aβ42 samples without D3 but huge amorphous structures without any ribbons or elongated fibrillar morphology in the D3 containing Aβ samples.

Recently, Aβ particles have been reported to have infectious properties. Minute amounts of material containing Aβ brought in direct contact with the CNS were shown to induce cerebral β-amyloidosis (*39*). The seeding capabilities of Aβ aggregates are discussed as important toxic and pathogenic properties. To investigate the in vitro seeding potential of D3-induced Aβ aggregates, we carried out seeding experiments (Figure 4C). Aβ only fibrils stimulated fibrillogenesis, whereas Aβ-D3 coaggregates did not, suggesting that Aβ-D3 coaggregates do not have a fibrillar or otherwise amyloidogenic structure. This is in accordance with the observation that Aβ-D3 coaggregates are negative for Congo red absorption and ThT fluorescence.

An additional insight into the mechanism of D3 action can be gleaned from computational studies of an Aβ-nonamer in the presence and absence of D3. The simulations, based on an experimentally determined Aβ structure (*40*), show that D3 is able to form strong interactions with negatively charged groups of Aβ. These interactions, which persist over the entire simulation time (Figure 5E,F), compensate the charge on the Aβ-surface and are therefore expected to reduce solubility and promote the aggregation of Aβ. This is consistent with the experimental observation of large nonfibrillar Aβ-aggregates in the presence of D3.

In addition, D3 binding also has an effect on the topology of the Aβ-oligomer itself. While the twist angle (Figure 5H) of the unliganded oligomer is approximately 5° between adjacent momomers (Figure 5C,D,G), D3 binding induces a twist of more than 12° (Figure 5E,F,G). In this context, it is interesting to note that the twist angle of 5° determined for the unbound oligomer is much larger than the value of 0.45° measured for Aβ42 fibrils (*40*). This observation suggests that Aβ-oligomers represent a much more suitable target for D3 binding than Aβ-fibrils for two reasons: (i) the initial twist of the oligomer is larger, which should facilitate D3 binding; and (ii) the conformational plasticity of the oligomer is higher, which allows it to tolerate the large twist induced by D3 binding. This large twist angle also locks the oligomers in a conformation, less suited to incorporation into fibrils, which are characterized by an extended conformation with a small twist angle. Therefore, also in silico, nonfibrillar aggregates are formed instead.

Our in vitro data clearly show that D3 precipitates toxic Aβ oligomers into large, high-molecular-weight, nontoxic, ThT negative, nonamyloidogenic amorphous aggregates that fail to act as seeds in Aβ fibril formation assays. It is important to stress the fact that in all assays, D3 did not increase the concentration of monomeric Aβ. Therefore, one possible mode of D3 action may be that the D3-induced conversion of Aβ species into amorphous Aβ-D3 aggregates adds an additional equilibrium to the complex network between the various Aβ species. D3 thereby shifts the equilibria among Aβ monomers, oligomers, and fibrils toward Aβ-D3 aggregates that are nonamyloidogenic and may be more amenable to degradation processes. Although D3 does not necessarily need to cross the blood−brain barrier (BBB) in order to do this, a cell culture model revealed D3 to cross the BBB significantly, indicating an adsorptive-mediated



DOI: 10.1021/cn100057j | ACS Chem. Neurosci. (2010), 1, 639–648

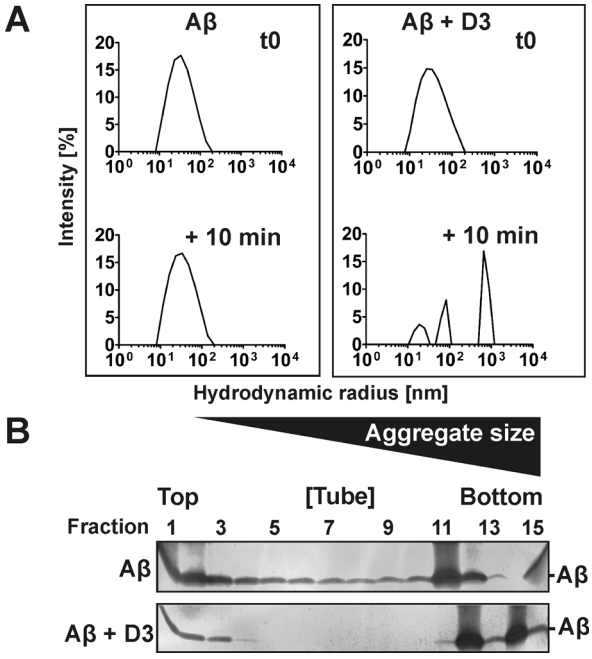


**Figure 3.** Aβ oligomer modulation by D3. (A) Particle size analysis by dynamic light scattering (DLS). Aβ and D3 as well as mixtures of both were prepared seedless in filtered sodium phosphate/NaCl buffer. DLS measurements were carried out at 20 °C, with a fixed angle (90°) and a cuvette path length of 3 mm. Data acquisition time was 1 s using a 655.6 nm (13 mW) laser. By using calculated autocorrelation functions, a regularization fit was performed in order to obtain size distribution profiles at $t = 0$ min (t0, upper row) and after 10 min (lower row). (B) Analysis of Aβ aggregation by density gradient ultracentrifugation. The size distributions of 125 μM Aβ42 and Aβ42-D3 mixtures (1:1) were determined by sedimentation analysis on a preformed gradient of iodixanol (Optiprep, AXIS-SHIELD, Oslo, Norway). One hundred microliters of aggregation assays containing 125 μM Aβ42 without or with 125 μM D3 was directly overlaid on a step gradient of 5−50% iodixanol. After centrifugation, 14 fractions from top to bottom of the centrifuge tube of 140 μL each were harvested. The 15th fraction represents the pellet. The fractions were analyzed by SDS−PAGE and silver staining.

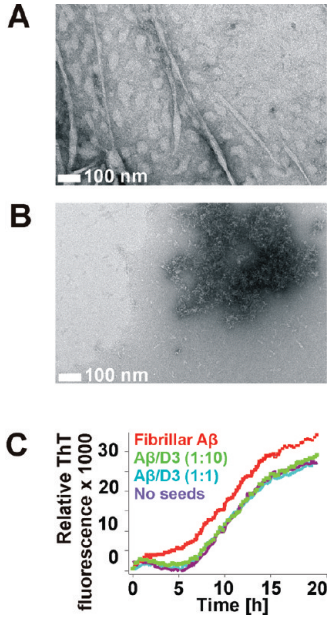


**Figure 4.** Analysis of amyloid properties of Aβ in the absence and presence of D3. (A and B) Electron micrographs of Aβ samples with and without D3. Twenty-five micromolar Aβ (A) and (1:4) Aβ-D3 (B) were negatively stained by uranyl acetate (1%) and measured as described in the Methods section. Scale bars: 100 nm. (C) Aβ fibril formation with and without seeds monitored by ThT fluorescence. Aβ only fibrils and Aβ-D3 coaggregates were prepared by incubating Aβ42 with and without different concentrations of D3 for 3 days at 37 °C. After washing, the precipitated seeds (20% v/v) were added to the aggregation reactions consisting of freshly prepared Aβ42 solutions. The relative ThT fluorescence of freshly prepared Aβ with fibrillar Aβ seeds (red), Aβ-D3 coaggregates (1:1, light blue), Aβ-D3 coaggregates (1:10, green), and freshly prepared Aβ as a control (purple) is shown as a function of time.

transcytosis mechanism (*41*), very similar to that reported for other arginin-rich proteins such as Tat (*42*).

In summary, we demonstrate that the mirror image phage display derived D-enantiomeric peptide D3 is able to reduce Aβ plaque load and enhance the cognitive state of transgenic AD mice even after oral application. D3 exerts an interesting and novel mechanism of action that abolishes toxic Aβ oligomers and thereby supports their decisive role in AD development and progression.

# Methods

## Peptides

D3 (RPRTRLHTHRNR, all amino acids are D-enantiomers) and Aβ(1−42) were purchased as reversed phase high performance liquid chromatography purified products (Jerini Biotools, Berlin, Germany).

## Seedless Aβ Stock Solutions

Aβ was dissolved in hexafluoroisopropanol (HFIP) to 1 mM and incubated overnight at room temperature. Stock solutions were aliquoted and stored at −20 °C until required. Prior to use, HFIP was evaporated. HFIP pretreated Aβ pellets were incubated in 100 mM NaOH, diluted in seedless buffer (50 mM sodium phosphate buffer, containing 100 mM NaCl, pH 7.5), and the pH value adjusted by the addition of 100 mM HCl.

## Thioflavin T (ThT) Assays

ThT assays were performed as described elsewhere (*32*) with minor modifications. Aβ aliquots and D3 were dissolved in PBS (140 mM NaCl, 2.7 mM KCl, 10 mM $Na_2HPO_4$, and 1.8 mM $KH_2PO_4$, pH 7.4) and added to a ThT solution (5 μM ThT, 50 mM Glycin, in NaOH−$H_2O$, pH 8.5). Samples were incubated at 37 °C.

## Congo Red Spectral Shift Assay

The amyloidogenic properties of Aβ aggregates were determined by the Congo red spectral shift assay according to Klunk et al. (*43*, *44*). Aggregates were formed as described for density gradient centrifugation either with or without the addition of equimolar (125 μM) amounts of D3 and diluted into PBS buffer, pH 7.4, to a 0.06 mg/mL final concentration of Aβ. A freshly prepared stock solution of Congo red was added to the solution to yield a 10 μM concentration. After 20 min of incubation at ambient temperature, absorption spectra from 700 to 300 nm were recorded using a V-650 UV−vis spectrophotometer (Jasco, Germany). As controls, the spectra of Congo red, ligand, and Aβ alone were recorded.



DOI: 10.1021/cn100057j | ACS Chem. Neurosci. (2010), 1, 639–648

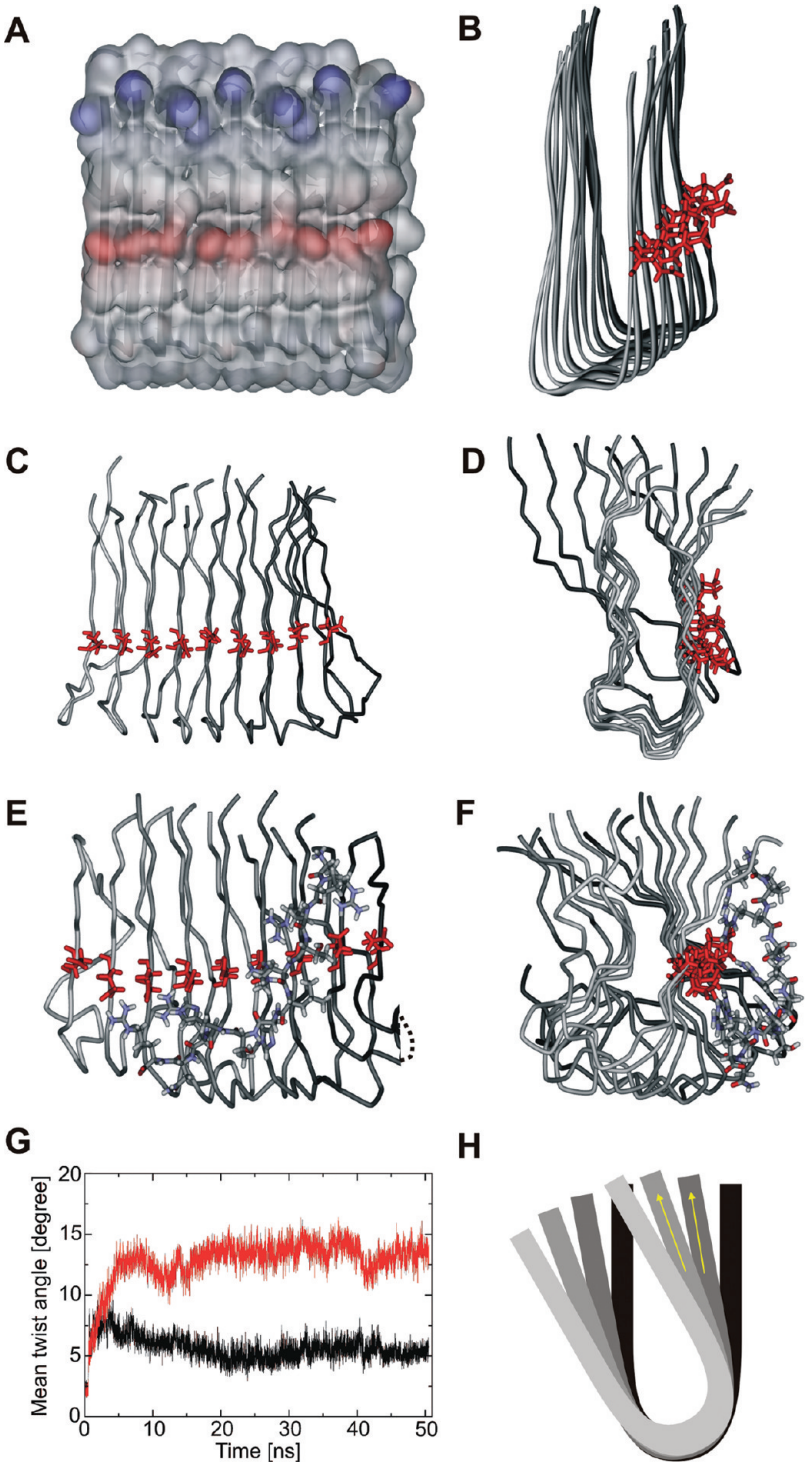


**Figure 5.** Computational analysis of the A$\beta$-D3 interaction. The initial structure of the A$\beta$(15−42) nonamer (A,B) and the structures of the unliganded nonamer (C,D) and the A$\beta$-D3 complex (E,F) after 50 ns of molecular dynamics simulations are shown as the top and side views, respectively. These two views differ by a rotation of approximately 90° around the vertical axis. The top layers of the oligomer are colored in light gray, and a color gradient is used for the lower layers of the oligomer. The electrostatic surface is shown for the initial structure in Figure 3A, in which the positive and negative surface charges originate from Lys16 and Glu22, respectively. Glu22 is shown as red sticks in panels B to F. D3 is shown in stick representation (colored according to the atom types) in panels E and F. A dotted line represents a disordered region of the terminal A$\beta$-chain. (G) Changes of the twist angle over the simulation time for the unliganded and D3-bound A$\beta$-oligomer. (H) Schematic presentation of a twisted A$\beta$-oligomer. The yellow arrows represents the vector between the C$\alpha$-carbons of Val18 and Val24. The angle between two vectors of adjacent chains was used to calculate the twist angle as described in the Methods section. Note the significantly enhanced twist angle in the D3-bound form (F) compared to the starting structure (B), which reflects the properties of the fibril.



DOI: 10.1021/cn100057j | *ACS Chem. Neurosci.* (2010), *1*, 639–648

The absorption spectrum of the Aβ in the absence of the dye was used to subtract the scattering contribution of the aggregates from the spectrum of the dye in their presence.

## Density Gradient Centrifugation

Density gradient centrifugation was performed according to Rzepecki et al (*25*). Preformed gradients of optiprep (Axis-Shield, Oslo, Norway) of about 2 mL volume were overlaid with 100 μL sample volumes, containing either 125 μM Aβ42 alone or an equimolar mixture of Aβ42 and D3. After centrifugation at 260,000*g* for 3 h at 4 °C in a TL100 ultracentrifuge (Beckman-Coulter, Palo Alto, USA) with aTLS-55 rotor, 14 fractions of 140 μL each were harvested from top to bottom. These fractions and the pellet of each tube were subsequently analyzed with respect to their Aβ42 content by denaturing, discontinuous Tris-Tricine-SDS−PAGE optimized for the separation of small peptides or proteins. Mark12 (Invitrogen, Germany) with molecular weights between 2500 and 200,000 Da was used as a size standard. The protein content was visualized by silver staining.

## Dynamic Light Scattering

Seedless Aβ as well as D3 were prepared in a seedless buffer. The buffer was filtered (0.22 μm pore size) prior to use. DLS measurements were carried out with a DynaPro DLS system (Protein Solutions, Lakewood, NJ, USA) at 20 °C, fixed angle (90°), and a cuvette path length of 3 mm. Data acquisition time was 1 s using a 655.6 nm (13 mW) laser. Analysis and averaging of the collected data was performed with the software Dynamic V6 (Protein Solutions). By using calculated autocorrelation functions, a regularization fit was performed in order to obtain the size distribution profile. The data were plotted using GraphPad Prism 5.01.

## Electron microscopy

Peptide aggregates were adsorbed on Formvar/carbon coated copper grids (Plano GmbH, Wetzlar), washed, and negatively stained with 1% uranyl acetate (pH 4.0). The grids were observed using a LaB6 CM12 EM (FEI/Philips), operating at 120 kV with a nominal magnification of 40,000×. Images were taken using an Orius 832 SC1000 CCD camera (4008 × 2672 pixels) (Gatan inc.).

## Seeding Assays

The assays were performed as already described (*23*) with minor modifications. As Aβ only seeds, lyophilized Aβ was predissolved in DMSO, diluted in PBS (phosphate buffered saline: 140 mM NaCl, 2.7 mM KCl, 10 mM $Na_2HPO_4$, and 1.8 mM $KH_2PO_4$, pH 7.4), and incubated (37 °C, 3 d). Aβ-D3-seeds were incubated in the presence of different amounts of D3. After incubation, the respective seeds were washed by centrifugation and redissolved in PBS. In the fresh samples without seeds, Aβ was also predissolved in DMSO. All samples were diluted in PBS to a concentration of 10 μM Aβ containing 100 μM ThT. Mixtures of 80% (v/v) freshly prepared Aβ and 20% (v/v) seeds or control samples were made. The measurements of seed containing samples were corrected by subtracting the ThT signal (fluorescence values) obtained for 20% (v/v) seeds.

## Computational Studies

A stack of nine Aβ(15−42)-monomers was generated on the basis of the experimental structural information about the geometry of Aβ42 in the fibrillar state (PDB code 2BEG) (*40*). This nonamer served as a model system for Aβ-oligomers in all subsequent computational studies. A candidate binding site of D3 was determined by inspecting the electrostatic potential of Aβ(15−42). The surface patch with the highest excess of negative charge is formed by the E22 side chains of adjacent Aβ subunits (Figure 5A). The positively charged side chains of D3 were therefore placed in spatial proximity of the E22 ladder. A 50 ns molecular dynamics (MD) simulation was performed to verify, whether this mode of interaction results in a stable complex. In addition, a control MD simulation was performed for the uncomplexed Aβ-nonamer. All simulations and data analysis were performed using standard protocols as described previously (*45*). The calculation of the twist angle followed the work of Zheng et al (*46*). For the calculation of the twist angle, vectors between Cα atoms of Val18 and Val24 were defined. The angle between vector pairs for consecutive Aβ-chains (omitting the first and last chain to account for boundary effects) was computed for all structures obtained from the MD simulation.

## Animals

APP and PS1 double transgenic mice (APPswe/PS1Δ*E*9 mice (*37*), $n = 12/17$) were used in the present study. The mice were acquired from JAX at the age of six weeks, and until the treatments, the animals were housed 4/cage in our facility, in a controlled environment (temperature 22 °C, humidity 50−60%, and light from 07:00−19:00); food and water were available ad libitum. The experiments were conducted in accordance with the local Institutional Animal Care and Use Committee (IACUC) guidelines.

## D3 Oral Treatment

The group (6 animals) of four-month old mice was treated for eight weeks with D3 via their drinking water. The peptide concentration was 1 mg/mL. On average, the mice drank ca. 0.5 to 1 mL water per day. The stability of D3 in water containing mouse spit was verified using reversed phase HPLC analysis. Seven weeks after the start of the treatment, the animals were tested in the water maze, and eight weeks after the start of treatment, the animals were sacrificed for histopathological analysis (see below).

## Brain Infusion

In parallel to the orally treated mice, 6 mice were treated with D3 via brain infusion. The applied D-peptide amount was 0.5 mg/pump. The Alzet minipump (model #2004; delivery rate: 0.25 μL/h; duration 8 weeks) was soaked in sterile saline for 24 h, and the next day the pump, the connecting tube and cannula (Alzet Brain Infusion Kit 3; Alzet) were filled with the appropriate solution, and they were connected such that no air bubbles were present. Then the cannulae were implanted in the brain (right dorsal hippocampus); in short, mice were anesthetized, placed in a stereotaxic frame, a hole was drilled above the right dorsal hippocampus, and the cannula was lowered into the hippocampus. The implantation of the cannula was in the dorsal hippocampus in all animals. The implantation of the Alzet minipumps did not change any obvious physiological parameters (e.g., growth as measured by body weight or general health) in the implanted mice or cause any noticeable discomfort, and none of the animals lost the brain cannula or developed any other problems. Seven weeks after start of the infusion period, the mice were behaviorally tested in the Morris water maze for one week. During this week, the



DOI: 10.1021/cn100057j | ACS Chem. Neurosci. (2010), 1, 639–648

treatment was continued. Subsequently, the animals were sacrificed for histopathological analysis (see below).

### Behavior

The animals were tested for one week in an open field water maze (*47*). Our version of the maze consisted of a blue circular tank of clear water (23 ± 1 °C). The mice were placed in the water at the edge of the pool and allowed to swim in order to locate a hidden, but fixed escape platform, using extra-maze cues. On Day 1, the mice were placed in the pool and allowed to swim freely for 90 s to find the hidden platform. If the animal did not locate the platform during that time, it was placed upon it by the experimenter and left there for 10 s. Each animal was tested in four trials per day. The intertrial interval was 60 s. There was no significant difference in the swimming speed between the groups of mice.

Each start position was used equally in a pseudorandom order, and the animals always placed in the water facing the wall. The platform was placed in the middle of one of the quadrants of the pool (i.e., northwest, southwest, northeast, or southeast; approximately 30 cm from the side of the pool). The mouse's task throughout the experiment was to find and escape onto the platform. Once the mouse had learned the task (Day 5, Trial 20), a probe trial was given immediately following the last trial of acquisition on Day 5. In the probe trial (i.e., Trial 21), the platform was removed from the pool and animals allowed to swim for 60 s.

Data were analyzed by Student's paired *t* test (treated versus nontreated) and by ANOVA (Systat 11; between groups), and posthoc tests (Tukey and Scheffe) were carried out to determine the source of a significant main effect or interaction.

### Histopathology

In short, the mice were anesthetized, transcardially perfused, and their brains removed. Following postfixation and cryoprotection, six series (1 in 6) of coronal sections were cut through the brain. The first series of sections was mounted unstained, the second, third, and fourth series were stained immunohistochemically according to published protocols (*48*), and the other two series were stored at −20 °C in antifreeze for future analysis. One half of the second series was stained for human Aβ using the W0−2 antibody (mouse antihuman Aβ4−9 (*49*)), and the other half of the second series was stained for mouse Aβ (rabbit antirodent Aβ, Covance (*48*)). The first half of the third series was immunohistochemically stained for Aβ40 (mouse anti-Aβ40, Covance) and the other half for Aβ42 (mouse anti-Aβ42, Covance). One half of the fourth series was stained for GFAP (mouse anti-GFAP; Sigma), whereas the other half was stained for CD11b (rat antimouse CD11b; Serotec), a marker of microglia. Some of these stained sections were double stained with Congo red, thioflavine S, or thiazine red. The sections destined for Aβ staining were pretreated for 30 min with hot (85 °C) citrate buffer. The series of sections were transferred to a solution containing the primary antibody; this solution consists of TBS with 0.5% Triton X-100 added (TBS-T) (*50*). Following incubation in this solution for 18 h on a shaker table at room temperature (20 °C) in the dark, the sections were rinsed three times in TBS-T and transferred to the solution containing the secondary antibody (goat antimouse·biotin; Sigma or sheep antirat Ig·biotin, Serotec). After 2 h, the sections were rinsed three times with TBS-T and transferred to a solution containing mouse ExtrAvidin (Sigma). Following rinsing, the sections were incubated for approximately 3 min with Ni-enhanced DAB (*50*). In a small number of sections, the Aβ deposits were double labeled for Aβ40, Aβ42, GFAP, or CD11b using fluorescent secondary antibodies. All stained sections were mounted on slides and coverslipped.

### Quantification

The appropriate areas (dorsal hippocampus and frontal cortex) of the brains were digitized using an Olympus DP70 digital camera, and the images were converted to gray scale using the Paint Shop Pro 7 program (*50*). To avoid changes in lighting, which might affect measurements, all images were acquired in one session. Furthermore, to avoid differences in staining density between sections, the measurements were performed on sections that were stained simultaneously, i.e., in the same staining tray ($n = 24$). The percentage of area covered by the reaction product to Aβ was measured (*48*) in the ipsi- and contralateral hippocampus and ipsi- and contralateral frontal cortex using the ScionImage (NIH) program (*50*). Employing a similar procedure, using digital images to overlay the defined measurement area, plaques were counted in the same brain area on the adjacent sections that were stained with Congo red. The density of GFAP or CD11b staining was measured by placing a standard sized circle (200 μm diameter) around the plaque core (stained with Congo red) and measuring the optical density of the staining in the circle using the ScionImage (NIH) program. All density measurements were done in triplicate, i.e., measuring the standardized area around three plaques at three different levels of the dorsal hippocampus and the frontal, midline cortex. These measurements were done blind in sections stained by an observer with no knowledge of the treatment of the animal (*50*). Data were analyzed by Student's paired *t* test (ipsi- versus contralateral) and by ANOVA (Systat 11; between groups), and posthoc tests (Tukey and Scheffe) were carried out to determine the source of a significant main effect or interaction.

## Supporting Information Available

Details of the stomach infusion experiments, SEC, dot blot analysis, ThT assays, turbidity assays, results of the transgenic animal studies in the Morris water maze assay, summary of important quantities, SEC analysis of 100 μM Aβ without and with FITC-labelled D3, and inhibition of ThT positive Aβ fibril formation. This information is available free of charge via the Internet at http://pubs.acs.org.

## Author Information

### Corresponding Author

* To whom correspondence should be addressed. ISB-3, Forschungszentrum Jülich, Wilhelm-Johnen Str., 52426 Jülich, Germany. Tel: +49 2461 61 2100. Fax: +49 2461 61 2233. E-mail: d.willbold@fz-juelich.de.

### Author Contributions

⊗ These authors contributed equally to this work.

S.A.F. and D.W. did the overal strategic planning and design of the study. S.A.F, D.B., L.N.-S., C.K., T.vG., and I.K.



DOI: 10.1021/cn100057j | ACS Chem. Neurosci. (2010), 1, 639–648

planned the details of the studies. S.A.F. and D.W. have written major parts of the manuscript. D.B., O.B. L.N.-S., T.S., G.S., C.K., A.M.-S., C.M., and R.B.-S. have designed and performed the in vitro studies. I.K. and T.vG. have designed and performed the in vivo studies. The molecular dynamics simulations were designed and done by A.H. and H.S. All authors have contributed to the manuscript text.

**Funding Sources**

This work has been supported by a grant from Volkswagen-Stiftung to D.W., C.K., and H.S. (I/82 649). Support from the "Präsidentenfond der Helmholtzgemeinschaft" (HGF, "Virtual Institute of Structural Biology") to D.W. is acknowledged. C.M. was supported by a DGCIS grant (French state). The electron microscopy facility used for this work is part of the Partnership for Structural Biology (PSB). Part of this research was supported by P30 NS47466. I.K. and T.v.G have been supported by 5P50 AG16582-10.

## References

1. Brookmeyer, R., Johnson, E., Ziegler-Graham, K., and Arrighi, H. M. (2007) Forecasting the global burden of Alzheimer's disease. *Alzheimer's Dementia 3*, 186–191.

2. Haass, C., and Selkoe, D. J. (1993) Cellular processing of beta-amyloid precursor protein and the genesis of amyloid beta-peptide. *Cell 75*, 1039–1042.

3. Kang, J., Lemaire, H. G., Unterbeck, A., Salbaum, J. M., Masters, C. L., Grzeschik, K. H., Multhaup, G., Beyreuther, K., and Muller-Hill, B. (1987) The precursor of Alzheimer's disease amyloid A4 protein resembles a cell-surface receptor. *Nature 325*, 733–736.

4. Weidemann, A., Konig, G., Bunke, D., Fischer, P., Salbaum, J. M., Masters, C. L., and Beyreuther, K. (1989) Identification, biogenesis, and localization of precursors of Alzheimer's disease A4 amyloid protein. *Cell 57*, 115–126.

5. Hardy, J. A., and Higgins, G. A. (1992) Alzheimer's disease: the amyloid cascade hypothesis. *Science 256*, 184–185.

6. Selkoe, D. J. (1991) The molecular pathology of Alzheimer's disease. *Neuron 6*, 487–498.

7. Haass, C., and Selkoe, D. J. (2007) Soluble protein oligomers in neurodegeneration: lessons from the Alzheimer's amyloid beta-peptide. *Nat. Rev. Mol. Cell Biol. 8*, 101–112.

8. Lambert, M. P., Barlow, A. K., Chromy, B. A., Edwards, C., Freed, R., Liosatos, M., Morgan, T. E., Rozovsky, I., Trommer, B., Viola, K. L., Wals, P., Zhang, C., Finch, C. E., Krafft, G. A., and Klein, W. L. (1998) Diffusible, nonfibrillar ligands derived from Abeta1−42 are potent central nervous system neurotoxins. *Proc. Natl. Acad. Sci. U.S.A. 95*, 6448–6453.

9. Shankar, G. M., Bloodgood, B. L., Townsend, M., Walsh, D. M., Selkoe, D. J., and Sabatini, B. L. (2007) Natural oligomers of the Alzheimer amyloid-beta protein induce reversible synapse loss by modulating an NMDA-type glutamate receptor-dependent signaling pathway. *J. Neurosci. 27*, 2866–2875.

10. Walsh, D. M., and Selkoe, D. J. (2007) A beta oligomers: a decade of discovery. *J. Neurochem. 101*, 1172–1184.

11. Blennow, K., de Leon, M. J., and Zetterberg, H. (2006) Alzheimer's disease. *Lancet 368*, 387–403.

12. Roberson, E. D., and Mucke, L. (2006) 100 years and counting: prospects for defeating Alzheimer's disease. *Science 314*, 781–784.

13. Jakob-Roetne, R., and Jacobsen, H. (2009) Alzheimer's disease: from pathology to therapeutic approaches. *Angew. Chem., Int. Ed. 48*, 3030–3059.

14. Nerelius, C., Johansson, J., and Sandegren, A. (2009) Amyloid beta-peptide aggregation. What does it result in and how can it be prevented? *Front. Biosci. 14*, 1716–1729.

15. Podlisny, M. B., Walsh, D. M., Amarante, P., Ostaszewski, B. L., Stimson, E. R., Maggio, J. E., Teplow, D. B., and Selkoe, D. J. (1998) Oligomerization of endogenous and synthetic amyloid beta-protein at nanomolar levels in cell culture and stabilization of monomer by Congo red. *Biochemistry 37*, 3602–3611.

16. McLaurin, J., Golomb, R., Jurewicz, A., Antel, J. P., and Fraser, P. E. (2000) Inositol stereoisomers stabilize an oligomeric aggregate of Alzheimer amyloid beta peptide and inhibit abeta -induced toxicity. *J. Biol. Chem. 275*, 18495–18502.

17. Townsend, M., Cleary, J. P., Mehta, T., Hofmeister, J., Lesne, S., O'Hare, E., Walsh, D. M., and Selkoe, D. J. (2006) Orally available compound prevents deficits in memory caused by the Alzheimer amyloid-beta oligomers. *Ann. Neurol. 60*, 668–676.

18. Gervais, F., Paquette, J., Morissette, C., Krzywkowski, P., Yu, M., Azzi, M., Lacombe, D., Kong, X., Aman, A., Laurin, J., Szarek, W. A., and Tremblay, P. (2007) Targeting soluble Abeta peptide with Tramiprosate for the treatment of brain amyloidosis. *Neurobiol. Aging 28*, 537–547.

19. Cherny, R. A., Atwood, C. S., Xilinas, M. E., Gray, D. N., Jones, W. D., McLean, C. A., Barnham, K. J., Volitakis, I., Fraser, F. W., Kim, Y., Huang, X., Goldstein, L. E., Moir, R. D., Lim, J. T., Beyreuther, K., Zheng, H., Tanzi, R. E., Masters, C. L., and Bush, A. I. (2001) Treatment with a copper-zinc chelator markedly and rapidly inhibits beta-amyloid accumulation in Alzheimer's disease transgenic mice. *Neuron 30*, 665–676.

20. Price, K. A., Crouch, P. J., and White, A. R. (2007) Therapeutic treatment of Alzheimer's disease using metal complexing agents. *Recent Pat. CNS Drug Discovery 2*, 180–187.

21. Necula, M., Breydo, L., Milton, S., Kayed, R., van der Veer, W. E., Tone, P., and Glabe, C. G. (2007) Methylene blue inhibits amyloid Abeta oligomerization by promoting fibrillization. *Biochemistry 46*, 8850–8860.

22. Bieschke, J., Russ, J., Friedrich, R. P., Ehrnhoefer, D. E., Wobst, H., Neugebauer, K., Wanker, E. E. EGCG remodels mature {alpha}-synuclein and amyloid-{beta} fibrils and reduces cellular toxicity, *Proc. Natl. Acad. Sci. U.S.A.*

23. Ehrnhoefer, D. E., Bieschke, J., Boeddrich, A., Herbst, M., Masino, L., Lurz, R., Engemann, S., Pastore, A., and Wanker, E. E. (2008) EGCG redirects amyloidogenic polypeptides into unstructured, off-pathway oligomers. *Nat. Struct. Mol. Biol. 15*, 558–566.

24. Nagel-Steger, L., Demeler, B., Meyer-Zaika, W., Hochdorffer, K., Schrader, T., and Willbold, D. (2010) Modulation of aggregate size- and shape-distributions of



DOI: 10.1021/cn100057j | *ACS Chem. Neurosci.* (2010), *1*, 639–648

the amyloid-beta peptide by a designed beta-sheet breaker. *Eur. Biophys. J. 39*, 15–22.

25. Rzepecki, P., Nagel-Steger, L., Feuerstein, S., Linne, U., Molt, O., Zadmard, R., Aschermann, K., Wehner, M., Schrader, T., and Riesner, D. (2004) Prevention of Alzheimer's disease-associated Abeta aggregation by rationally designed nonpeptidic beta-sheet ligands. *J. Biol. Chem. 279*, 47497–47505.

26. Juhasz, G., Marki, A., Vass, G., Fulop, L., Budai, D., Penke, B., Falkay, G., and Szegedi, V. (2009) An intraperitoneally administered pentapeptide protects against Abeta (1−42) induced neuronal excitation in vivo. *J. Alzheimer's Dis. 16*, 189–196.

27. Poduslo, J. F., Curran, G. L., Kumar, A., Frangione, B., and Soto, C. (1999) Beta-sheet breaker peptide inhibitor of Alzheimer's amyloidogenesis with increased blood-brain barrier permeability and resistance to proteolytic degradation in plasma. *J. Neurobiol. 39*, 371–382.

28. Soto, C., Sigurdsson, E. M., Morelli, L., Kumar, R. A., Castano, E. M., and Frangione, B. (1998) Beta-sheet breaker peptides inhibit fibrillogenesis in a rat brain model of amyloidosis: implications for Alzheimer's therapy. *Nat. Med. 4*, 822–826.

29. Tjernberg, L. O., Naslund, J., Lindqvist, F., Johansson, J., Karlstrom, A. R., Thyberg, J., Terenius, L., and Nordstedt, C. (1996) Arrest of beta-amyloid fibril formation by a pentapeptide ligand. *J. Biol. Chem. 271*, 8545–8548.

30. Frydman-Marom, A., Rechter, M., Shefler, I., Bram, Y., Shalev, D. E., and Gazit, E. (2009) Cognitive-performance recovery of Alzheimer's disease model mice by modulation of early soluble amyloidal assemblies. *Angew. Chem., Int. Ed. 48*, 1981–1986.

31. van Groen, T., Kadish, I., Wiesehan, K., Funke, S. A., and Willbold, D. (2009) In vitro and in vivo staining characteristics of small, fluorescent, Abeta42-binding D-enantiomeric peptides in transgenic AD mouse models. *ChemMedChem 4*, 276–282.

32. van Groen, T., Wiesehan, K., Funke, S. A., Kadish, I., Nagel-Steger, L., and Willbold, D. (2008) Reduction of Alzheimer's disease amyloid plaque load in transgenic mice by D3, a D-enantiomeric peptide identified by mirror image phage display. *ChemMedChem 3*, 1848–1852.

33. Wiesehan, K., Buder, K., Linke, R. P., Patt, S., Stoldt, M., Unger, E., Schmitt, B., Bucci, E., and Willbold, D. (2003) Selection of D-amino-acid peptides that bind to Alzheimer's disease amyloid peptide abeta1−42 by mirror image phage display. *ChemBioChem 4*, 748–753.

34. Wiesehan, K., Stohr, J., Nagel-Steger, L., van Groen, T., Riesner, D., and Willbold, D. (2008) Inhibition of cytotoxicity and amyloid fibril formation by a D-amino acid peptide that specifically binds to Alzheimer's disease amyloid peptide. *Protein Eng., Des. Sel. 21*, 241–246.

35. Schumacher, T. N., Mayr, L. M., Minor, D. L. Jr., Milhollen, M. A., Burgess, M. W., and Kim, P. S. (1996) Identification of D-peptide ligands through mirror-image phage display. *Science 271*, 1854–1857.

36. Van Regenmortel, M. H., and Muller, S. (1998) D-peptides as immunogens and diagnostic reagents. *Curr. Opin. Biotechnol. 9*, 377–382.

37. Jankowsky, J. L., Slunt, H. H., Ratovitski, T., Jenkins, N. A., Copeland, N. G., and Borchelt, D. R. (2001) Co-expression of multiple transgenes in mouse CNS: a comparison of strategies. *Biomol. Eng. 17*, 157–165.

38. Lafaye, P., Achour, I., England, P., Duyckaerts, C., and Rougeon, F. (2009) Single-domain antibodies recognize selectively small oligomeric forms of amyloid beta, prevent Abeta-induced neurotoxicity and inhibit fibril formation. *Mol. Immunol. 46*, 695–704.

39. Eisele, Y. S., Bolmont, T., Heikenwalder, M., Langer, F., Jacobson, L. H., Yan, Z. X., Roth, K., Aguzzi, A., Staufenbiel, M., Walker, L. C., and Jucker, M. (2009) Induction of cerebral beta-amyloidosis: intracerebral versus systemic Abeta inoculation. *Proc. Natl. Acad. Sci. U.S.A. 106*, 12926–12931.

40. Luhrs, T., Ritter, C., Adrian, M., Riek-Loher, D., Bohrmann, B., Dobeli, H., Schubert, D., and Riek, R. (2005) 3D structure of Alzheimer's amyloid-beta(1−42) fibrils. *Proc. Natl. Acad. Sci. U.S.A. 102*, 17342–17347.

41. Liu, H., Funke, S. A., Willbold, D. (2010) Transport of alzheimer disease amyloid-beta-binding d-amino acid peptides across an in vitro blood-brain barrier model, *Rejuvenation Res. 13*, 210−213.

42. Rapoport, M., and Lorberboum-Galski, H. (2010) TAT-based drug delivery system: new directions in protein delivery for new hopes? *Expert Opin. Drug Delivery 6*, 453–463.

43. Klunk, W. E., Jacob, R. F., and Mason, R. P. (1999) Quantifying amyloid by congo red spectral shift assay. *Methods Enzymol. 309*, 285–305.

44. Klunk, W. E., Jacob, R. F., and Mason, R. P. (1999) Quantifying amyloid beta-peptide (Abeta) aggregation using the Congo red-Abeta (CR-abeta) spectrophotometric assay. *Anal. Biochem. 266*, 66–76.

45. Kassler, K., Horn, A. H., Sticht, H. (2010) Effect of pathogenic mutations on the structure and dynamics of Alzheimer's Abeta(42)-amyloid oligomers, *J. Mol. Model. 16*, 1011−1020.

46. Zheng, J., Jang, H., Ma, B., Tsai, C. J., and Nussinov, R. (2007) Modeling the Alzheimer Abeta17−42 fibril architecture: tight intermolecular sheet-sheet association and intramolecular hydrated cavities. *Biophys. J. 93*, 3046–3057.

47. Handattu, S. P., Garber, D. W., Monroe, C. E., van Groen, T., Kadish, I., Nayyar, G., Cao, D., Palgunachari, M. N., Li, L., and Anantharamaiah, G. M. (2009) Oral apolipoprotein A-I mimetic peptide improves cognitive function and reduces amyloid burden in a mouse model of Alzheimer's disease. *Neurobiol. Dis. 34*, 525–534.

48. van Groen, T., Kiliaan, A. J., and Kadish, I. (2006) Deposition of mouse amyloid beta in human APP/PS1 double and single AD model transgenic mice. *Neurobiol. Dis. 23*, 653–662.

49. Ida, N., Hartmann, T., Pantel, J., Schroder, J., Zerfass, R., Forstl, H., Sandbrink, R., Masters, C. L., and Beyreuther, K. (1996) Analysis of heterogeneous A4 peptides in human cerebrospinal fluid and blood by a newly developed sensitive Western blot assay. *J. Biol. Chem. 271*, 22908–22914.

50. Kadish, I., Pradier, L., and van Groen, T. (2002) Transgenic mice expressing the human presenilin 1 gene demonstrate enhanced hippocampal reorganization following entorhinal cortex lesions. *Brain Res. Bull. 57*, 587–594.



DOI: 10.1021/cn100057j | *ACS Chem. Neurosci.* (2010), *1*, 639–648